DETERMINATION OF SPECIFIC INTERFACIAL AREAS IN SWIRLED TWO-PHASE FLOW

Kurt WINKLER[a], František KAŠTÁNEK[b] and Jan KRATOCHVÍL[b]

[a] *Central Institute of Physical Chemistry, Academy of Sciences of the GDR, 1199 Berlin GDR and*
[b] *Institute of Chemical Process Fundamentals, Czechoslovak Academy of Sciences, 165 02 Prague 6 - Suchdol, ČSSR*

Received October 17th, 1980

Specific gas–liquid interfacial area in flow tubes 70 mm in diameter of the length 725 and 1 450 mm resp. containing various swirl bodies were measured for concurrent upward flow in the ranges of average gas (air) velocities 11 to 35 ms^{-1} and liquid flow rates 13 to 80 $m^3 m^{-2} h^{-1}$ using the method of CO_2 absorption into NaOH solutions. Two different flow regimes were observed: slug flow and swirled annular-mist flow. In the latter case the determination was carried out separately for the film and spray flow components, respectively. The obtained specific areas range between 500 to 20 000 $m^3 m^{-2}$. Correlation parameters are energy dissipation criteria, related to the geometrical reactor volume and to the static liquid volume in the reactor.

Detail understanding of complex two-phase flow processes has been steadily gaining importance in chemical engineering. The use of stream tubes in mass transfer equipments shows a possible way for intensification of such processes. The main advantages are high through-puts at little dimensions of the contacting elements. The additional swirling of phases allows the combination of transfer and separation processes in a single element. Multistage devices can be then formed combinating such elements. Some work has been already done in this field devoted to such fundamental problems as minimization of pressure drop, ways of raising separation degree of the fluids, development of transfer equipment including economic studies and also concerning the scale up of test apparatus including comparison with industrial-scale data[1–5].

However, much work is still to be done to clarify fundamentals of exchange mechanism, such as connection of hydrodynamics and mass transfer coefficients. Mechanisms of dispersion and coalescence at high flow rates is also to be studied as well as the relations between surface characteristics and the transfer effectivity. Progress in solving the above stated problems has been severely hampered by the lack of data on specific interfacial area.

The main goal of the present work has been the determination of the specific interfacial area as a function of various geometrical factors and process variables and data correlation with recommendations for practical use.

To obtain the data on specific interfacial area the chemical method of CO_2 absorption into alkali solutions was used described *e.g.* by Danckwerts[6]. The obtained data were correlated with the pressure drop, the phase separation degree and hold-up parameters in the form of energy dissipation plots.

Values of the specific interfacial area were determined under conditions of pseudo first-order reaction kinetics by plotting

$$(j/c^*_{CO_2}a)^2 = f(D_{CO_2}k_2c_{NaOH} + k_L^2) \qquad (1)$$

with the criteria

$$M = (\pi/4)\, k_2 c_{NaOH} t \qquad (2)$$

$$N = 1 + c_{NaOH}/c^*_{CO_2} \qquad (3)$$

$$H = p_{CO_2}/C^*_{CO_2} \qquad (4)$$

$$m\sqrt{M} = N\,. \qquad (5)$$

EXPERIMENTAL

The experiments were carried out in the apparatus shown in Fig. 1. Various apparatus variants and experimental conditions are summarized in Table I.

Operation variables were: $140 \leqq \dot{V}_{GE}$ ($m^3\ h^{-1}$) $\leqq 480$, $13 \leqq \dot{Q}_{LE}$ ($m^3\ m^{-2}\ h^{-1}$) $\leqq 80$, $\dot{V}_{CO_2,E} \leqq 3{\cdot}5\ m^3\ h^{-1}$, max. 1·4 vol. % according Eq. (5) with factor $m = 1{-}6$; $c_{NaOH,E} = 0{\cdot}05{-}0{\cdot}5$ kmol m^{-3}.

The measurements were conducted at room temperature with adjustment of the liquid to the air temperature. All throughputs were measured by normalized blends resp. recalibrated rotameters in the usual way. The determination of CO_2 concentration was carried out as follows: 1 ml probes of NaOH, containing absorbed CO_2, dissolved in hot H_2SO_4 (20%). The released CO_2 was led after together with a H_2 carrier gas through a conductivity cell. The measured, digitalized and integrated current was compared with that of decomposed standard $KHCO_3$ probes. The NaOH concentrations were determinated titrimetrically against phenolphthalcine.

TABLE I

Basic experimental variants, 70 mm internal diameter of the tube

Code	h mm	$V_R \cdot 10^3$ m^3	Direction of liquid inlet	Swirl body arrangement
A_K[a]	725	4·62	toward the	under liquid entry
A_L	1 450	7·39	tube head	under liquid entry
B_L	1 450	7·51	downward	above liquid entry
C_L	1 450	7·51	downward	without swirl body

[a] Blade angle of the swirl bodies (from the horizontal) $\alpha = 30$, 44·5, 50·5, 58·5, 73 ; for other variants only $\alpha = 58{\cdot}5°$.

Care was taken to protect the probes from uncontrolled mass transfer in the collecting zones. All gas volumes over the probe levels were washed carefully by nitrogen.

The (second) swirl body in the spray separator was omitted in determinations of the spray specific interfacial area to avoid additional mass transfer; it was needed only to obtain the mass balances. The constants D_{CO_2}, H, k_2 (Eq. (*1*) and (*4*)) were corrected to the temperature and the ionic strength.

It has been found in preliminary laminar-jet absorption experiments that the data by Brož[7] gave somewhat (c. 15%) better agreement than Pohorecki's[8] data.

In swirled two-phase flow there exists a significant radial pressure gradient. It seemed to be doubtful, whether the pressure readings on wall chamber give representative values of cross sectional average pressures. We have proved, using a Pitot tube, that at reasonable stream tube lengths ($h/d \geqq 10$) and at reasonable liquid loads the pressure measured on the wall differs by max. 30% from the average value. Further details on the pressure correction will be published elsewhere[9]. In preliminary experiments we also selected such conditions that the film and spray volume parts did not depend considerably on geometry and on dimensions of the film separator slit. The upper swirl body was adjusted to give optimal spray separation, too.

Varying NaOH concentrations while keeping all the other parameters constant, we have observed some irregularities. The interfacial tension influences the structure of two-phase flow,

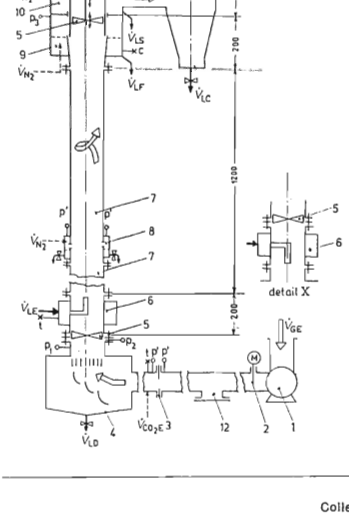

FIG. 1

Experimental arrangement with two phase flow tube 1 Gas blower, 2 slide valve, 3 normalized blend, 4 column bottom with training blades, 5 swirl body, 6 liquid inlet section, 7 measure section, 8 chambers for pressure drop measurements and concentration probes, 9, 10 film and spray separator, 11 cyclone, 12 tap for hold-up measurements, p, p′ taps for pressure drop measurements, t thermometer. For the detail X see Table I

which becomes finer and tends to foam at increased concentrations. However, this effect was within limits of the experimental error ($\pm 15\%$) and was therefore neglected.

The hold-up data were obtained by measurement of the drain rates $\dot{V} - \dot{\gamma}\ \dot{V}_{LE}$ realizing an air by-pass by the high speed trap 12 (Fig. 1). Fig. 2 shows a typical hydraulic operation diagram. Regime borders were: *a*) at low gas velocities and low liquid loads — the conditions for suspending droplets in the vertical directed flow; *b*) at still smaller gas velocities and higher liquid loads — the weeping through the swirl body blades; *c*) at higher gas velocities and higher liquid loads — the liquid separation degree; *d*) at both high loads — the flooding conditions.

Regimes

According to the specifications given above there exist two regimes: *1*) at lower gas velocities a transition regime of unstable slug flow and *2*) at higher gas velocities a transition regime to the pure swirled annular — mist flow. As the character in the slug flow regime is complicated, it is not logical to distinguish there further between film and spray regime. In this region the mass transfer rate j (Eq. (*I*)) was estimated as a product of analytic concentration reading and the over-all liquid throughput, $j = q\dot{V}_{LE}$. In the case of pure annular flow it is reasonable to base the

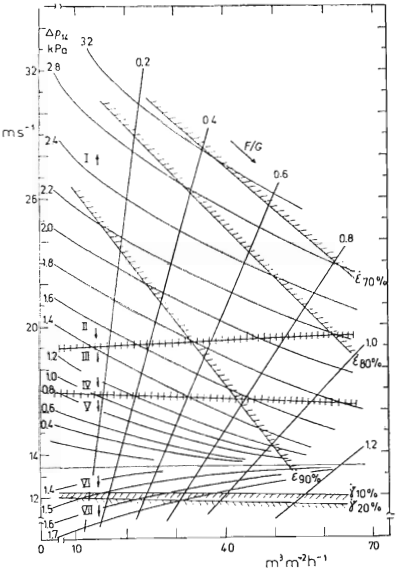

FIG. 2

Operation diagram of variant A_K (Table I). $\bar{w}_G$ mean gas velocity, $m\,s^{-1}$, $\dot{V}_{GE}$ gas throughput, $m^3\,s^{-1}$, $\dot{V}_{LE}$ liquid throughput, $m^3m^{-2}\,h^{-1}$. Parameters: pressure drop over the whole flow section Δp_{14} (Fig. 1), kPa; ranges of various flow regimes; degrees of 70, 80 and 90% separation of the inlet liquid rate $\dot{\varepsilon}$; limits of raining down 10% and 20% of the liquid $\dot{\gamma}$; the liquid–gas mass ratio L/G. Observed flow regime (beginning from the most intensive one): I swirled annular-mist ring-spray) flow with thin liquid film stresses on tube wall; II stable swirled annular-mist flow; III unstable swirled annular flow, partially destroyed in the upper tube parts; IV thrusting flow with some whirls in lower tube parts; V unstable wispy-annular flow with rest whirls and strong vertical oscillatory motions; VI partially rotating slug flow over the swirl body; VII raining down of the liquid

estimation of j on the separate film and spray throughputs $\dot{V}_{LF} = \varepsilon_F \dot{V}_{LE}$ and $\dot{V}_{LS} = \varepsilon_S \dot{V}_{LE}$ respectively.

In the correlations we also distinguished between the film and the spray pressure drops, Δp_{13} and Δp_{14} (Fig. 1). However, it was not always possible to use only average gas velocities as correlation parameters; in these cases the factor

$$f = 1{\cdot}04(1 - 0{\cdot}89 \sin \alpha) \qquad (6)$$

was introduced, stemming from geometrical considerations[9].

The influence of the liquid phase mass transfer coefficient in Eq. (5) could be neglected due to its value lower by two orders of magnitude.

RESULTS AND DISCUSSION

The dependence of specific interfacial area on energy dissipation criterion was observed for all the tube variants, but it was influenced by the choice of the throughput and volume variables. Examples of dependence for various A_K are shown in Fig. 3. For average gas flow rates above 12 m s^{-1} partially rotating swell flow regime was observed in the lower part of the tube, with high liquid hold-up and consequently with large residence time and intensive internal recirculation. The specific interfacial area, related to the reactor volume as a fundamental variable, were of the order up to 20 000 m^2 m^{-3}. Raising gas velocities brought hold-up decrease. With "free--blowing" of the swirl body the specific interfacial area decreased and consequently a stable swirled annular flow was built up. The minimum was reached at $\bar{w}_G = 16$ to 19 m s^{-1}. For higher $\bar{w}_G$ values the specific interfacial area increased, due to the

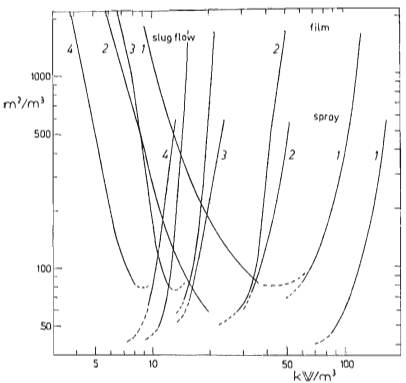

FIG. 3

Principal dependences of specific interfacial area related to reactor volume, a/V_R (m^2 m^{-3}), on the energy dissipation criterion E_G/V_R (kW m^{-3}) at the specific liquid load, $\dot{Q}_{LE} = 19{\cdot}8$ m^3 m^{-2} h^{-1} for variants A_K. Parameter: blade angle 1 $\alpha = 30°$, 2 $\alpha = 44{\cdot}5°$, 3 $\alpha = 58{\cdot}5°$, 4 $\alpha = 73°$. The curves represent data concerning the two regimes slug flow and annular-mist flow (Fig. 2) with the film and the spray component

high turbulent stress forces in the wall film. Up to $\bar{w}_G \leqq 35$ m s^{-1} no plateau could be observed on the a/V_R dependence. The data on both falling branches of the graph can be better correlated using variables containing the static liquid volume based on liquid hold-up. It confirmed Kasturi's[10] conclusion on suitable data fits for pronounced disperse flow. With f after (6) as geometrical correction factor, a satisfactory correlation of all data for the slug flow regime was reached as shown in Fig. 4. An additional dependence on the ratio F/G still remains.

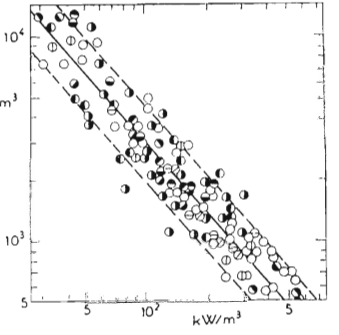

FIG. 4

Specific interfacial area for the slug flow, related to the liquid volume, a/V_L, m^2 m^{-3} on the modified gas energy dissipation criterion $(F/G)^{0.85}\,(E_G/V_L)\,f^{0.20}$, kW m^{-3}, for all variants after Table II. For bodies see Fig. 5

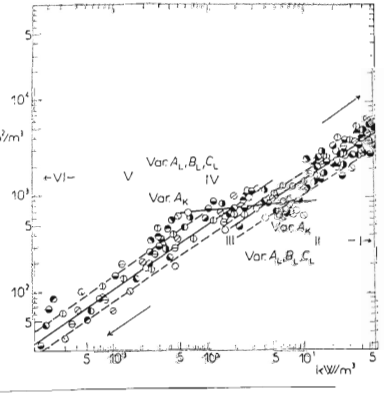

FIG. 5

Specific interfacial area for the film flow related to V_L, a_F/V_L (m^2 m^{-3}) depending on the film energy dissipation criterion E_{LF}/V_L, kW m^{-3}, with various regimes. The top dart until $a_F/V_L = 20\,000$ m^{-1}, the low dart until $a_F/V_L = 4$ m^{-1}

It should be mentioned that other dependent parameters as shown in Fig. 3 could describe only slightly better the relations of the specific interfacial area. The parameters on operation are *i.e.* $\psi_{TB} = \psi_T(1 + (\dot{V}_0/\dot{V}_L))$ (ref.[11]) and $\psi_{TP} = \psi_T - \bar{\varrho}\bar{w}_{LE}$, where $\bar{\varrho}$ is the mean density, based on corresponding phase volumes[16] or mass throughputs[18] of single pases,

$$\bar{\varrho}_V = \bar{\varphi}_L\varrho_L + \bar{\varphi}_G\varrho_G \tag{7}$$

resp. $\bar{\varrho}_{\dot{m}} = \bar{\varphi}_L\varrho_L + \bar{\varphi}_G\varrho_G$. The best results however can be obtained for data plots of the form a/V_R *vers.* ψ_{TP} after (7). Similarly to[19], the curves exhibit low maximum, minimum and an inflection point. The observed ranges correspond to the slug, intermediate and annular flow regime, respectively.

In the examination of the film areas, the liquid film volume was preferred as the fundamental variable. It yielded a fit better by several orders as shown in Fig. 5. Three ranges can be distinguished in the graph, corresponding to main flow regimes. In the lower part of the graph, the dependence of slug flow data is analogous to those in Fig. 3, however with more convenient coordinates. This region corresponds to complete mixing. The specific interfacial area for the slug flow has to be, therefore, the same as for the film flow which represents only a negligible vertically transported amount of the liquid phase ($a_F = \dot{\varepsilon}_F a$). The upper part of the graph describing the annular flow has a similar slope, it is however, shifted in the vertical direction. Regarding constant specific amounts of dissipated energy in liquid volume we can conclude that in annular flow (in composition with swell flow) no significant recirculation takes place which can be explained by the increase of effective film area.

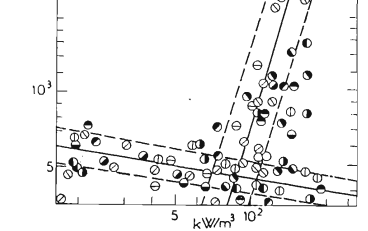

FIG. 6

Specific interfacial area for the spray flow related to V_L, a_S/V_L ($m^2\ m^{-3}$) on the modified gas energy dissipation criterion $E_G/(V_R f^{0.30})$, $kW\ m^{-3}$. For bodies see Fig. 5 (but instead of A_K $\alpha = 30°$, A_L $\alpha = 44{\cdot}5°$, B_L $\alpha = 58{\cdot}5°$, C_L $\alpha = 73°$). The dart until $a_S/V_L = 10\,000\ m^{-1}$

TABLE II

Specific interfacial areas a/V_R determined by chemical methods in equipment, working preferably in annular-mist flow regime

Equipment	d mm	Length m	$\bar{w}_G$ m s^{-1}	$\dot{Q}_{LE}$ m^3 m^{-2} s^{-1}	a/V_R m^2 m^{-3}	Reference
Whole absorber without elements	80–385	0·6–3	0·25–0·35	6·7–75	12–100	12
Venturi absorber	20[a]		25–50	0·008–25	400–2 000	13
Forced spray absorber	20[a]		18–35	6–115	200–700	14
Vertical tube	6	1·52	0·5–13	250–1 830	120–1 000	10
Horizontal tube	25·4		40–60	445–2 220	400–2 500	15
Helical coil	16·5	13·9–15·1	0·5–36	100–7 400	250–500	16
Helical coil	16·5	2·0	0·5–36	100–7 400	150–700	17
Vertical tube	10; 18; 24	4·0	1·6–22	1 100–1 480	1 100–50 000	18
Vertical tube with swirl body	70	0·72–1·46	12–35	13–80	500–20 000	present work

[a] Nozzle diameters.

With some caution, it is possible to correlate the data in the intermediate flow regime range, too. Fig. 6 shows also correlation of the spray-regime data (obtained only for the A-variants). Decisive variables are the reactor volume and the gas throughput. This seems to be logical as the droplets move preferably in the swirled gas core. In the annular – mist flow regime the strong increase of the specific interfacial area with energy losses is clearly apparent. The growing macroscopic geometrical interface cannot be solely responsible for them because the dispersion degree of droplets increases to certain plateau value with raising loads of both fluid phases. Convective forces are further to be considered causing intensive additional small oscillations on droplets with rigid sphere behaviour due to the high tangential shear stress forces. In the intermediate regime no such a substantial dependence exists. Regarding the smaller phase velocities, formation of larger droplets with lower integral areas can be expected.

Previously published works devoted to determination of the specific interfacial area values are summarized in Table II. The data were obtained in various contact devices working mostly in the regime of disperse flow of the liquid phase. Whereas our results are partly of the same order as those obtained in other intensive-contact devices, somewhat higher values of a/V_R (up to 20 000 $m^2 m^{-3}$) were obtained in the swirled-flow region as a result of increased contact distance and load capacity per unit volume. However, it is apparent from Table III that in high-velocity contacting equipments only a smaller part of the input gas phase energy is spent for the interfacial area formation. Predominant part of energy is lost for the liquid phase motion (especially in phase separation processes) and for uncontrolled turbulent dissipations.

TABLE III

Interfacial areas a related to the energy consumption from the gas stream for some mass transfer equipment

Equipment	a, $m^2 kW^{-1}$	Reference
Tubular jet reactor	500—3 000	19
Bubble column	1 000—1 700	19
Bubble column with recirculation	850—1 400	20
Jet reactor	60— 800	19
Flow tube	50— 70	10
Venturi	1— 10	19
Flow tube with swirl body	2— 100	present work

TABLE IV

Values of main correlation parameters according to Eq. (7) for various mass transfer equipments

Equipment	Variables Eq. (7)	A	m	$Re_G \cdot 10^{-4}$ [a]	Regime	Reference
Tube with swirl body	a_F, V_L, E_{LF}	2 710	0·5	4 – 9	annular flow	present work
		3 830	0·5	9 – 16		
Packing column	a, V_R, E_G	—	0·4	0·05 – 5	cocurrent bubble flow	21
Tubular jet reactor	a, V_{nozzle}, E_G	—	0·4	0·04 – 0·8	forced bubbling	
Jet reactor	a, V_R, E_G	—	0·82	0·005 – 0·3	forced bubbling	
Venturi absorber	a, V_R, E_G	—	0·4 – 0·7	20 – 100	annular-mist flow	
Tube with swirl body	a, V_L, E_G	$2{\cdot}2 \cdot 10^6 (F/G)^{0{\cdot}85}$	−1·15	4 – 7·5	slug flow	present work
	a_S, V_R, E_G	$1{\cdot}9 \cdot 10^{-4} f^{-2}$	3·2	9 – 16	spray flow	
	a_F, V_L, E_{LF}	1 140	0·2	7·5 – 9	intermediate flow	
	a_S, V_R, E_G	950	−0·2	7·5 – 9	intermediate flow	

[a] Estimation based on main stream zone parameters.

Compared with other correlations of the type

$$(a/V) = A(E/V)^m \tag{8}$$

the obtained exponent m as a film flow parameter is in a good agreement with literature data (Table IV). It appears that the energy needed for the formation of interfacial area per unit volume is derived in swirled flow tubes preferably from the liquid phase. This seems to be reasonable because the pressure drop was measured on the wall and therefore represents mainly the energy dissipation in the film.

The high velocity flow tubes with swirl bodies have been therefore proved to be suitable mass transfer devices in which sufficiently high specific interfacial areas can be performed.

The authors wish to thank to Dr Z. Šir and to Dr M. Minárik for helpful advice and assistance in analytical work.

LIST OF SYMBOLS

A	coefficient, defined by Eq. (7)
a	interfacial area m^2
c	concentration kmol m^{-3}
D	diffusion coefficient $m^2\ s^{-1}$
d	diameter m
E	energy flow kW
F/G	liquid to gas mass ratio —
f	geometrical factor, defined by Eq. (6)
h	height m
H	Henry coefficient Nm $kmol^{-1}$
j	mass transfer rate kmol s^{-1}
k	mass transfer coefficient $m\ s^{-1}$
k_2	reaction rate constant $m^3\ kmol^{-1}\ s^{-1}$
M, N, m, n	coefficients, def. by Eqs (2), (3), (5), (7)
p	pressure $N\ m^{-2}$
Δp	pressure drop $N\ m^{-2}$
Q	specific volume $m^3\ m^{-2}$
t	contact time s
V	volume m^3
w	velocity $m^3\ s^{-1}$
z	stoechiometric coefficient —
α	swirl body blade angle degree
γ	raining down rate —
ε	liquid separation degree —
φ	hold-up —
ϱ	density kg m^{-3}

Indices

E inlet
G gas
L liquid
F film
S spray
R reactor
TP two-phase flow
T total
$*$ interfacial
$-$ mean
$\cdot$ time related

Complexes

$E_G = \Delta p_{14} \dot{V}_G f^{-1}$ kW
$E_{LF} = \Delta p_{13} \dot{V}_{LF}$ kW
$\psi = \Delta p_{13} \dot{V}_L V_R^{-1}$ kW m^{-3}

REFERENCES

1. CISE-Rep. No 002-59-11 RDJ, A Research Programm in Two-phase Flow, Milano 1963.
2. Uspenski V. A., Kiselev V. M.: Teor. Osn. Khim. Tekhnol. *8*, 428 (1974).
3. Nikolaev N. A., Zhavoronkov N. M.: Teor. Osn. Khim. Tekhnol. *4*, 261 (1970); *7*, 386 (1973).
4. Nikolaev N. A., Zhavoronkov N. M., Malyusov V. A.: Teor. Osn. Khim. Tekhnol. *8*, 853 (1973).
5. Plechov J. M., Levdonski E. J., Jershov A. J., Ivanov V. A.: III. Vsesoyuz. Konfer. Teorii Praktike Rektifikacii, Severodonetzk 1973, Part II, p. 283.
6. Danckwerts P. V.: *Gas–Liquid Reactions*. McGraw-Hill, New York 1970.
7. Brož Z.: Private communication.
8. Pohorecki R., Moniuk W.: Inz. Chem. *5*, 569 (1975).
9. Winkler K.: Unpublished results.
10. Kasturi G., Stepanek J. B.: Chem. Eng. Sci. *29*, 713 (1974).
11. Jepsen J. C.: AIChE J. *16*, 705 (1970).
12. Metha K. C., Sharma M. M.: Brit. Chem. Eng. *15*, 1556 (1970).
13. Filatov N. N., Matrosov V. I.: Tr. Khim. Khim. Tekhnol. (Gorkii) 1970, Nr. 2, 196.
14. Tshagina Z. V., Ramm V. M., Ternovskaya A. M.: Trudy NIUIF Im. Samoylova, 1970, Nr. 214, 76.
15. Wales C. E.: AIChE J. *12*, 1166 (1966).
16. Banerjee S., Scott D. S., Rhodes E.: Can. J. Chem. Eng. *48*, 542 (1970).
17. Kulic E., Rhodes E.: Can. J. Chem. Eng. *52*, 114 (1974).
18. Tomida T., Yusa F., Okazaki T.: Chem. Eng. J. *16*, 81 (1978).
19. Nagel O., Kürten H., Sinn R.: Chem.-Ing.Tech. *44*, 899 (1972).
20. Hirner W.: *Thesis*, University Stuttgart, 1974.
21. Nagel O., Kürten H., Hegner B.: Chem.-Ing.-Tech. *45*, 913 (1973).

Translated by M. Rylek.